

Low-Temperature Non-Ohmic Galvanomagnetic Effects in Degenerate n -Type InAs[†]

G. Bauer and H. Kahlert

Ludwig Boltzmann-Institute für Festkörperphysik

and Institut für Angewandte Physik der Universität Wien, A-1090 Vienna, Austria

(Received 12 July 1971)

The dependence of the mobility of n -InAs on temperature and electric field was measured between 4.2 and 30 K and 0.05 and 10 V/cm, respectively. Furthermore, the variation of the nonoscillatory as well as the oscillatory part of the magnetoresistance (Shubnikov-de Haas effect) with applied electric field was studied experimentally. It was found that the decrease of the amplitudes of the Shubnikov-de Haas (SdH) effect depends on the time after application of the electric field and allows a direct time-resolved observation of the increasing electron temperature. The non-Ohmic transport is interpreted with the aid of an electron-temperature model. At electric fields below 0.3 V/cm, where the electron gas is strongly degenerate, electron temperatures are deduced from the decreases of the SdH amplitudes. At higher fields the degeneracy decreases gradually and electron temperatures are obtained from a comparison of the field-dependent non-Ohmic mobility and the temperature-dependent Ohmic mobility. From energy-balance considerations, the dependences of the electron temperature and the mobility on the electric field strength are calculated up to 10 V/cm assuming that ionized-impurity scattering is the dominant mechanism for momentum relaxation. The energy loss was assumed to involve scattering by acoustic phonons via the screened deformation potential and the screened piezoelectric interaction, and also scattering by polar optical phonons. A value of 4.05 eV for the deformation potential constant yielded good agreement between the experimental and the calculated dependence of the energy-loss rate on the electron temperature up to 18 K. Above 18 K the energy loss because of polar optical phonons, which is calculated for a degenerate electron gas, dominates the increase of the electron temperature and leads to a kink in the mobility-field characteristic. The nonoscillatory positive magnetoresistance is shown to be dependent on the electric field. The negative magnetoresistance of the samples under investigation was studied between 2.4 and 4.2 K. A semiempirical relation of the form $\Delta\rho/\rho_0 = -B_1 \ln[1 + B_2(T)B^2]$ was used to analyze the data.

I. INTRODUCTION

The study of hot-electron effects in III-V compounds has been the subject of a large number of papers.¹ Considerable effort has been devoted to the investigation of high-field transport in n -InSb²⁻⁹ and n -GaAs¹⁰⁻¹² at low temperatures. The main purpose of most of this work was the investigation of the momentum- and energy-loss mechanisms of the electrons to the lattice.

The comparison between the experimental results and the theoretical predictions has to overcome the difficulty that the energy distribution function of the carriers under non-Ohmic conditions cannot be deduced directly from transport experiments. Therefore one has to solve the Boltzmann equation for various types of scattering mechanisms. An alternative method is to assume a certain type of distribution function and to obtain a calculated mobility-field characteristic from momentum- and energy-balance considerations. If the assumed distribution function is a Maxwellian or a Fermi-Dirac distribution with the only adjustable parameter being the electron temperature T_e , which is higher than the lattice temperature T_L , this model is called the "electron-temperature model."¹³ The use of this model was favored by many authors be-

cause of its simplicity and its surprisingly good results.^{5,6,8} However, it was pointed out by Stratton¹³ that it is applicable only for semiconductors with high carrier concentrations where interelectronic collisions are frequent enough to establish the described type of distribution function.

If the assumption of the electron-temperature model is justified for the interpretation of a non-Ohmic transport experiment, one has to look for a method to determine the electron temperature experimentally. At low temperatures the dominant momentum-relaxation process of the electrons in most of the III-V compounds is ionized impurity scattering, which has no explicit dependence on the lattice temperature, but only on the mean carrier energy. Therefore, it is only necessary to determine the variation of the mobility with lattice temperature and to compare these data with the variation of the mobility with electric field at a fixed low temperature. In nondegenerate semiconductors this comparison yields directly the electron temperature. For highly doped materials, where the electron gas is degenerate, this method cannot be applied, since in the limit of strong degeneracy the mobility does not depend on the lattice temperature and therefore also not on the electron temperature. For this reason, a method which deter-

mines directly the electron temperature is more suitable to study hot-electron effects in degenerate semiconductors than the observation of the variation of the conductivity with electric field. The sensitivity of quantum oscillations like the Shubnikov-de Haas (SdH) effect has been suggested by Isaacson and Bridges¹⁴ for a study of degenerate *n*-InSb. This method has been adopted by Konopka¹⁵ for a study of *n*-InAs using a microwave technique. The present authors have reported an investigation of the oscillatory magnetoresistance of *n*-InAs using a pulsed dc technique.¹⁶

It is the purpose of this paper to give a detailed analysis of the Ohmic and non-Ohmic transport in degenerate *n*-InAs at temperatures between 4.2 and 30 K. For electric fields below 0.3 V/cm, electron temperatures are deduced from electric-field-dependent measurements of the amplitudes of the SdH oscillations. Because of the fact that the energy relaxation time τ_e is of the order of 10^{-7} sec, direct evidence for a variation of the electron temperature with time after application of a dc pulse is presented. Results of a negative magnetoresistance and the nonoscillatory positive magnetoresistance will be given and compared with data obtained under Ohmic conditions.

In Sec. II, we review the theory of the transport in a degenerate semiconductor with dominant impurity scattering including the Ohmic mobility and the Hall-coefficient factor r . Furthermore, we discuss the theory of the SdH effect as far as necessary for the interpretation of our measurements and review the theory of the negative and the nonoscillatory positive magnetoresistance. Finally, we collect the energy-loss rates for both types of screened acoustic scattering and for polar optical scattering considering degenerate statistics. In Sec. III, the experimental techniques are described. In Sec. IV, the results of the measurements are presented and their interpretation in terms of an electron-temperature model is given. In Sec. V, we present calculations of the energy-loss rates and of the field dependence of the electron temperature and the mobility.

II. THEORY

A. Ohmic Mobility and Hall Constant

Since the minimum carrier concentration in bulk *n*-InAs crystals is about 1×10^{16} cm⁻³, ionized impurity scattering dominates the low-temperature transport. Because the optical-phonon density decreases rapidly at low temperatures, polar optical-phonon scattering is weak below approximately 60 K. In the temperature range investigated here acoustic-phonon scattering has a negligible influence on the momentum relaxation compared with impurity scattering. For ionized impurity scatter-

ing, the mobility is given by the Brooks-Herring expression for a singly ionized impurity¹⁷

$$\mu_0^I(\eta) = \frac{2F_2(\eta)}{F_{1/2}(\eta)} \frac{\sqrt{2} \kappa^2 (kT_e)^{3/2}}{\pi e^3 m^{1/2} N_I g(\bar{x}_{1,\eta})}, \quad (1)$$

where N_I is the total impurity density, κ is the dielectric constant, m is the effective mass, k is Boltzmann's constant, T_e is the electron temperature, and $\eta = \epsilon_F/kT_e$, ϵ_F being the Fermi energy. F_k are the Fermi-Dirac integrals

$$F_k(\eta) = \int_0^\infty \frac{x^k dx}{e^{x-\eta} + 1}, \quad (2)$$

where $x = \epsilon/kT_e$, ϵ being the electron energy. $\bar{x}_{s,\eta}$ is determined by the condition

$$[\bar{x}_{s,\eta} - \frac{3}{2}(s+1)] = [\bar{x}_{s,\eta} + \frac{3}{2}(s+1)] e^{\eta - \bar{x}_{s,\eta}}, \quad (3)$$

and

$$g(\bar{x}_{s,\eta}) = \ln(1+z) - z/(1+z), \quad (4)$$

where

$$z = \frac{4\kappa m (kT_e)^2}{\pi e^2 \hbar^2 n} \frac{F_{1/2}(\eta)}{F_{-1/2}(\eta)} \bar{x}_{s,\eta}. \quad (5)$$

The screening density is assumed to be the free-carrier density n in the conduction band and s is an integer. This treatment is valid for $z \gg 1$.

A theoretical expression of the Hall-coefficient factor $r(\eta)$ for ionized impurity scattering is given by Beer,¹⁷

$$r_0^I(\eta) = \frac{3}{4} \frac{F_{7/2}(\eta) F_{1/2}(\eta) g^2(\bar{x}_{1,n})}{F_{3/2}(\eta) g^2(\bar{x}_{2,n})}. \quad (6)$$

In the limit of strong degeneracy $\eta \gg 20$, $r_0^I(\eta)$ approaches unity.

B. Oscillatory Magnetoresistance

With the application of a magnetic field the quasi-continuous distribution of energy levels in the conduction band is split into Landau-level subbands whose spacing is equal to $\hbar\omega_c$, where ω_c is the cyclotron frequency. Changes in the magnetic field result in a passage of the Landau levels past the Fermi energy. As a result, oscillations in the magnetic susceptibility and in transport properties such as magnetoresistance occur which are periodic as a function of the reciprocal magnetic field. The conditions necessary for the oscillatory effects to be observed are the following:

$$\omega_c \tau \gg 1, \quad \hbar\omega_c > kT_e, \quad \epsilon_F > \hbar\omega_c, \quad (7)$$

where $\omega_c = eB/m$; B represents the magnetic field, τ the relaxation or quantum-state lifetime, and ϵ_F the Fermi energy for zero magnetic field.

The theory of the transverse magnetoresistance for spherical energy surfaces and for both acoustic-phonon and ionized impurity scattering has been developed by Adams and Holstein.¹⁸ The relative amplitudes for both mechanisms are essentially the same. The theory of the longitudinal

oscillatory magnetoresistance has first been given by Argyres.¹⁹ The theoretical expressions are

$$\frac{\Delta\rho}{\rho_0} = a \sum_{s=1}^{\infty} \left[b_s \cos\left(\frac{2\pi s \epsilon_F}{\hbar\omega_c} - \frac{\pi}{4}\right) + R \right], \quad (8)$$

with

$$b_s = \frac{(-1)^s}{\sqrt{s}} \left(\frac{\hbar\omega_c}{\epsilon_F}\right)^{1/2} \frac{2\pi^2 s k T / \hbar\omega_c}{\sinh(2\pi^2 s k T / \hbar\omega_c)} \times \cos(\pi\nu s) e^{-2\pi^2 k T_D / \hbar\omega_c}, \quad (9)$$

where ρ_0 is the zero-field resistivity, s is the s th harmonic, ν is the ratio of the spin splitting to the Landau-level spacing, and T_D is the nonthermal broadening temperature. This temperature is called the Dingle temperature²⁰ and is related to the collision-broadening relaxation time τ_c by $T_D = \hbar/\pi k \tau_c$. The term R in Eq. (8) represents an additional series of oscillatory terms in the transverse magnetoresistance which is generally much smaller than the term b_s and vanishes in the longitudinal case. The factor a is equal to 2.5 or 1 in the transverse and longitudinal magnetoresistance, respectively.

Under the assumption of a constant Dingle temperature, the ratio of the amplitudes A of the oscillations at two different electron temperatures is given by

$$\frac{A(T_{e,1})}{A(T_{e,2})} = \frac{\chi_1/\sinh\chi_1}{\chi_2/\sinh\chi_2}, \quad (10)$$

where

$$\chi_i = 2\pi^2 k T_{e,i} / \hbar\omega_c.$$

C. Nonoscillatory Magnetoresistance

1. Negative Magnetoresistance

The phenomenon of negative magnetoresistance is well known in elemental semiconductors such as Ge²¹ and Si,²² but also in III-V compounds like GaAs²³ and InSb²⁴ at low temperatures. According to a theory by Toyozawa,²⁵ this negative magnetoresistance is caused by the existence of localized magnetic moments. He introduced a scattering process like s - d exchange interactions by noting the similarities between the negative magnetoresistance in semiconductors and in Cu-Mn alloys.²⁶ It was suggested that because of the statistical fluctuations in donor density and correlation effects, some electrons could be localized at donor sites giving rise to a localized magnetic moment similar to that of the Mn ions in Cu-Mn alloys.

In contrast to Ge and Si, the conduction in n -InAs does not take place in an impurity band but rather in the conduction band even at low temperatures. The impurity band probably does not exist independent from the conduction band²⁷ in samples with a carrier concentration of about 10^{16} cm⁻³. Although the Toyozawa model was developed for Ge, where

the existence of localized magnetic moments in an impurity band was shown theoretically, Katayama and Tanaka²⁴ applied this model successfully to a study of n -InSb where also no split-off impurity band was found for concentrations higher than 10^{14} cm⁻³. The Toyozawa concept provides at least a qualitative explanation for the observed concentration and temperature dependence: The negative magnetoresistance decreases for increasing carrier concentration and increases as the temperature decreases.

The magnetic scattering of the conduction electrons from the localized moments yields a decrease in resistivity proportional to the square of the average magnetization M of the localized spin system:

$$-\Delta\rho/\rho_0 \propto M^2. \quad (11)$$

This scattering process has to be independent of the direction of the magnetic field because the s - d interaction is isotropic. The above result is based on a second-order-perturbation calculation. A magnetoresistance coefficient S is defined by²¹

$$S = \lim_{B \rightarrow 0} \frac{\Delta\rho}{\rho_0 B^2}. \quad (12)$$

By plotting $(-S)^{1/2}$ vs T_L a Curie-Weiss law is obtained:

$$(-S)^{1/2} \propto C/(T_L + T_0), \quad (13)$$

where T_0 is a characteristic temperature and C is a constant.

However, it was pointed out by Khosla and Fischer²⁸ that such a procedure implies a saturation of the negative component of the magnetoresistance which cannot be shown directly because of the positive component. For strongly degenerate semiconductors this positive component should be zero if it is caused by the normal magnetoresistance. Khosla and Fischer pointed out that the second-order-perturbation theory is not sufficient for a description of the negative magnetoresistance and suggested that third-order terms should be included in the calculation of the s - d interaction. A semi-empirical relation was derived having the form

$$\Delta\rho/\rho_0 = -B_1 \ln[1 + B_2(T) B^2], \quad (14)$$

where B_1 and $B_2(T)$ are products of various constants given by Khosla and Fischer.²⁸

2. Positive Magnetoresistance

In the limit of weak magnetic fields ($\mu B \ll 1$), the transverse magnetoresistance for predominant ionized impurity scattering and arbitrary degeneracy is given by¹⁷

$$\frac{\Delta\rho}{\rho_0} = \left[\frac{2F_5(\eta) g^3(\bar{x}_{1,\eta})}{F_2(\eta) g^3(\bar{x}_{3,\eta})} - \left(\frac{3F_{7/2}(\eta) g^2(\bar{x}_{1,\eta})}{2F_2(\eta) g^2(\bar{x}_{2,\eta})} \right)^2 \right]$$

$$\times \left(\frac{\omega_e \tau_i}{g(\bar{x}_{1,n})} \right)^2, \quad (15)$$

with

$$\tau_i^0 = \frac{\kappa^2 (2m)^{1/2} (kT_e)^{3/2}}{\pi e^4 N_I}. \quad (16)$$

D. Energy-Loss Rates

In order to get information on the dominant energy-loss mechanisms the experimentally determined energy-loss rate P per electron has to be calculated. For both types of acoustic scattering we use the expressions derived by Greene²⁹ and Kogan.³⁰ For piezoelectric scattering, P is given by

$$\langle P_{pt} \rangle = \frac{16\pi (ee_{14})^2 (2m)^{3/2} k^{1/2}}{5\hbar^2 \kappa^2 d} \frac{T_e - T_L}{\sqrt{T_e}} \frac{F_0(\eta)}{F_{1/2}(\eta)}, \quad (17)$$

where e_{14} is the piezoelectric modulus and d is the mass density. The energy-loss rate per electron due to deformation potential scattering can be expressed according to Kogan³⁰ as

$$\langle P_{def} \rangle = \frac{(2m)^{5/2} k^{3/2} E_c^2}{\pi d \hbar^4} (\sqrt{T_e}) (T_e - T_L) \frac{F_1(\eta)}{F_{1/2}(\eta)}, \quad (18)$$

where E_c is the deformation potential constant. Both expressions for the energy-loss rates given by Eqs. (17) and (18) do not include the effect of conduction-electron screening on the electron-phonon interaction. If these effects are considered, $F_0(\eta)$ in Eq. (17) has to be replaced by

$$G_0(\eta) = \int_0^\infty \frac{x^2 dx}{(x+x_D)^2 (1+e^{x-\eta})} \quad (19)$$

and $F_1(\eta)$ in Eq. (18) by

$$G_1(\eta) = \int_0^\infty \frac{x^3 dx}{(x+x_D)^2 (1+e^{x-\eta})}, \quad (20)$$

as shown by Szymanska and Maneval.⁸ x_D is given by

$$x_D = \frac{\pi n e^2 \hbar^2}{16 m \kappa (kT_e)^2} \frac{F_{-1/2}(\eta)}{F_{1/2}(\eta)}. \quad (21)$$

For the case of polar optical scattering, Conwell's expression for the energy loss of a nondegenerate electron gas¹ has to be modified for Fermi-Dirac statistics. The Pauli exclusion principle leads to a factor $1 - f(\epsilon \pm \hbar\omega_0)$, which is equal to the probability that the final state of a scattered carrier is not occupied. $\hbar\omega_0$ is the optical-phonon energy. Because of the high value for the ratio of the Debye temperature Θ to the lattice temperature, the absorption of optical phonons by the electrons can be neglected in our case. The energy-loss rate is determined by the spontaneous-emission

process only and given by

$$P_{po} = \frac{2eE_0 \hbar\omega_0}{(2m\epsilon)^{1/2}} (N_q + 1) [1 - f(\epsilon - \hbar\omega_0)] \times \ln \left[\left(\frac{\epsilon}{\hbar\omega_0} \right)^{1/2} + \left(\frac{\epsilon}{\hbar\omega_0} - 1 \right)^{1/2} \right], \quad (22)$$

where E_0 is the coupling constant defined by¹

$$E_0 = \frac{me\hbar\omega_0}{\hbar^2} \left(\frac{1}{\kappa_\infty} - \frac{1}{\kappa} \right), \quad (23)$$

f is the Fermi-Dirac distribution function, N_q is the phonon distribution, and κ_∞ is the optical dielectric constant. This equation has to be averaged over the Fermi-Dirac distribution function to get the mean energy-loss rate per electron:

$$\langle P_{po} \rangle = \frac{\sqrt{2} e E_0 \hbar\omega_0}{(mkT_e)^{1/2} F_{1/2}(\eta)} \int_y^\infty f(x) [1 - f(x-y)] \times \ln \left[\left(\frac{x}{y} \right)^{1/2} + \left(\frac{x}{y} - 1 \right)^{1/2} \right] dx, \quad (24)$$

where $y = \Theta/T_e$ and $\hbar\omega_0 = k\Theta$.

III. EXPERIMENTAL

Samples were prepared from an n -type bulk single crystal of InAs having an electron concentration n of $2.5 \times 10^{16} \text{ cm}^{-3}$ and a mobility of 25 000 $\text{cm}^2/\text{V sec}$ at 4.2 K. The samples were oriented in a $\langle 100 \rangle$ direction. Typical sample dimensions were $0.5 \times 0.5 \times 7 \text{ mm}^3$. Two current and two potential contacts, and in some cases two Hall contacts, were soldered with tin to the samples. They were either directly immersed into liquid helium or placed within a variable-temperature cryostat for measurements between 2.4 and 30 K. Low-field Hall and magnetoresistance measurements were made by using a Keithley 148 nanovoltmeter. Pulsed-current techniques were used to avoid sample heating at high electric fields. Voltage pulses of 2- μsec duration, a repetition rate of 30 Hz, and rise times below 3 nsec were produced by discharging a coaxial cable through a mercury wetted relay. In order to observe any variation of the conductivity with electric field, with magnetic field, and with time after the application of the voltage pulse, two Tektronix sampling oscilloscopes (561B, 3S1, 3T2 and 561A, 3S76, 3T77) were used. The output signals were fed into an HP 7004 recorder. Using this x - y recorder and the field sweep of a superconducting coil, direct plots of the magnetoresistance vs B were obtained. The high-electric-field experiments were made under constant-current conditions. Pulsed Hall-effect measurements were performed using a Tektronix 556 real-time oscilloscope with a type-W differential-comparator unit. Reproducible and consistent re-

sults were obtained from a set of nine different samples cut from the same crystal. All results given in Sec. IV are taken from the representative sample B7.

IV. RESULTS AND ANALYSIS

A. Ohmic Conductivity and Hall Effect

The conductivity and Hall effect were measured between 2.5 and 77 K. From the fact that the Hall-coefficient factor r ($R_H = r/ne$) is equal to 1 for strongly degenerate semiconductors regardless of the scattering mechanisms, the carrier concentration and the conductivity mobility could be deduced from Hall and conductivity measurements at 4.2 K, where the reduced Fermi energy of sample B7 is 37.5.

Figure 1 shows the temperature dependence of the mobility and of the Hall constant R_H between 2.5 and 30 K. The small increase in R_H (measured at a magnetic field of 500 G) for increasing temperature is consistent with the assumption of a temperature-independent carrier density and reflects the influence of the temperature-dependent Hall-coefficient factor r . Because of the increasing temperature the reduced Fermi energy decreases, which in turn causes the Hall-coefficient factor to become larger.

In Fig. 1, the full line represents the results of a calculation using Eq. (1). The total impurity density was determined from a best fit of the theoretical curve to the experimental data and found to be $6.37 \times 10^{16} \text{ cm}^{-3}$. The Hall and mobility data do not exhibit any evidence for impurity conduction or donor ionization in the temperature range 4.2–77 K. The experimental data can be explained on the basis of a single-band model.

From measurements of the temperature dependence of the Hall coefficient R_H between 4.2 and 300 K, Zotova *et al.*³¹ came to the conclusion that there exists an impurity band in InAs of comparable carrier concentration. We feel, however, that their observed increase of the Hall coefficient R_H is caused by the increase of r and is no indication for two-band conduction. The increasing temperature removes the degeneracy and r increases from the value of 1 in the strongly degenerate case to the value of 1.93 in the nondegenerate case for ionized impurity scattering. The subsequent decrease of R_H above 77 K reflects simply the decrease of r , as lattice scattering becomes the dominating process for momentum relaxation.

We want to emphasize that in InAs of comparable carrier concentration, Kaufman and Neuringer²⁷ deduced from their high-magnetic-field Hall-coefficient data an appreciable overlap between the broadened impurity centers and the conduction-band tails. Since for such a complex conduction mechanism a calculation taking into account the

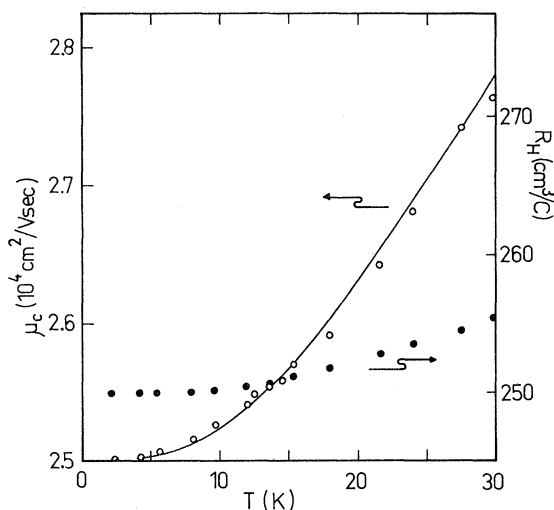


FIG. 1. Temperature dependence of the Ohmic conductivity mobility and of the Hall coefficient; open circles: experimental mobility; full line: calculated mobility; full circles: experimental Hall coefficient.

different mobilities of electrons in the states of the tail is not yet available, we have done the above simplified calculations and only within these reservations is our analysis justified.

B. Non-Ohmic Mobility

Figure 2 shows the variation of the conductivity with electric field for different lattice temperatures of 4.2, 15.5, and 31 K. The data were taken at the end of a 2- μ sec pulse. The curves for 4.2 and 15.5 K show an initially steep increase in the conductivity between 200 and 500 mV/cm followed by a region of smaller slope. Measurements in this field-strength region do not show any significant variation of the Hall constant R_H . Consequently this increase in conductivity cannot be attributed to either impact ionization of electrons frozen out on donor levels or to impact ionization of electrons from an impurity band.⁵ Therefore we conclude that this increase reflects a mobility change.

Figure 3 shows recorder tracings of the current density vs field strength up to 1 V/cm for a lattice temperature of 4.2 K. The different curves were taken at 30, 90, and 150 nsec after the rise of the current pulse. Although it is tempting to attribute the time-dependent variation of the conductivity to an ionization process, the Hall-effect data rule out this interpretation. Moreover, we will show in Sec. V that as in the case of InSb⁶ at comparable temperatures this time dependence of the conductivity is due to the influence of the energy-relaxation time of the order of 10^{-7} sec.

To analyze these data we use the electron-temperature model. This is justified because of the high carrier concentration of our samples which

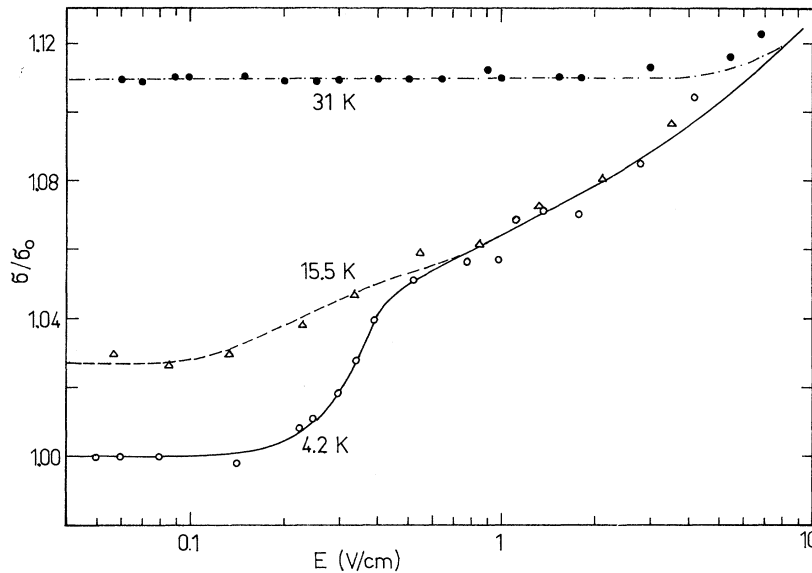


FIG. 2. Electric field dependence of the conductivity normalized to Ohmic conductivity at 4.2 K; open circles: $T_L = 4.2$ K; triangles: $T_L = 15.5$ K; full circles: $T_L = 31$ K; the curves are calculated ones for the respective temperatures.

enables the electron-electron scattering to be frequent enough to randomize energy and momentum. With this simple model the electron temperature which corresponds to a certain electric field can be determined experimentally by a comparison of the $\mu(E)$ and $\mu(T_L)$ curves as shown in Fig. 4. Below 200 mV/cm, the accuracy of our mobility measurements was not sufficient to draw conclusions about the electron temperature in this range of electric fields. Below 300 mV/cm, electron temperatures will be deduced from the decrease of the SdH amplitudes with electric field. A theoretical calculation of the dependences of the electron temperature and the mobility on the electric field will be given in Sec. V.

C. Oscillatory Magnetoresistance

Magnetic fields above 5 kG were sufficient to allow a measurement of the SdH effect in our samples. Figure 5 shows the variation of the longitudinal magnetoresistance with magnetic field up to 25 kG. The applied electric field for this measurement was below 5 mV/cm to ensure Ohmic conditions. Application of higher electric fields caused damping of the oscillations in the longitudinal as well as in the transverse magnetoresistance. The left-hand side of Fig. 6 shows the dependence of the transverse magnetoresistance on the applied electric field between 60 and 300 mV/cm. The right-hand side of Fig. 6 shows the time-dependent variation of the amplitudes of the SdH effect for different times between 15 nsec and 1.9 μ sec after the application of the voltage pulse corresponding to an electric field of 230 mV/cm. Depending on this time, the amplitudes decrease first rapidly and finally reach a saturation value which

manifests itself in a time independence of the magnetoresistance effect. Such curves were taken for a large number of applied electric fields between 2 and 300 mV/cm. Higher electric fields were not used for the SdH measurements since the mobility data of Fig. 2 show an appreciable increase of the mobility above this electric field. In Fig. 7, the variation of the oscillatory part of the longitudinal magnetoresistance under Ohmic conditions and for lattice temperatures between 4.2 and 12.5 K (left-hand side) is compared with measurements for different electric fields ranging from 2 to 320 mV/cm at a fixed lattice temperature of 4.2 K

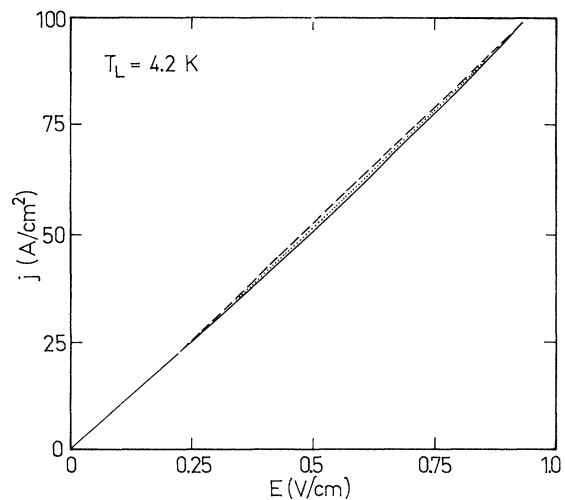


FIG. 3. j - E characteristic for different times after application of the voltage pulse; full line: 30 nsec after rise of the pulse; dotted line: 90 nsec; dashed line: 150 nsec.

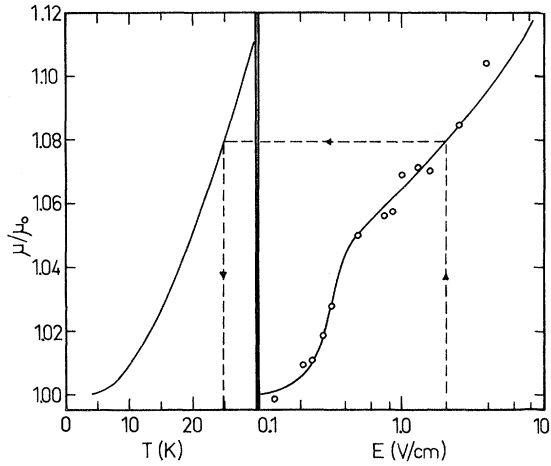


FIG. 4. Determination of the electron temperature which corresponds to a certain electric field from a comparison of the $\mu(T_L)$ and $\mu(E)$ curves.

(right-hand side). The equivalent effect of the increasing lattice temperature and of the rise of the electron temperature due to the application of an electric field is evident from this figure.

To deduce quantitatively the dependence of the electron temperature on the electric field strength from the decrease of the SdH amplitudes it is necessary to determine the Dingle temperature by the usual plot of $(AB^{-1/2} \sinh \chi) / \chi$ vs $1/B$ as shown in Fig. 8. From the data of Fig. 5, one obtains the data indicated by the open circles in Fig. 8. From the slope of the solid line, a Dingle temperature of 7.0 K was deduced. The open triangles in Fig. 8

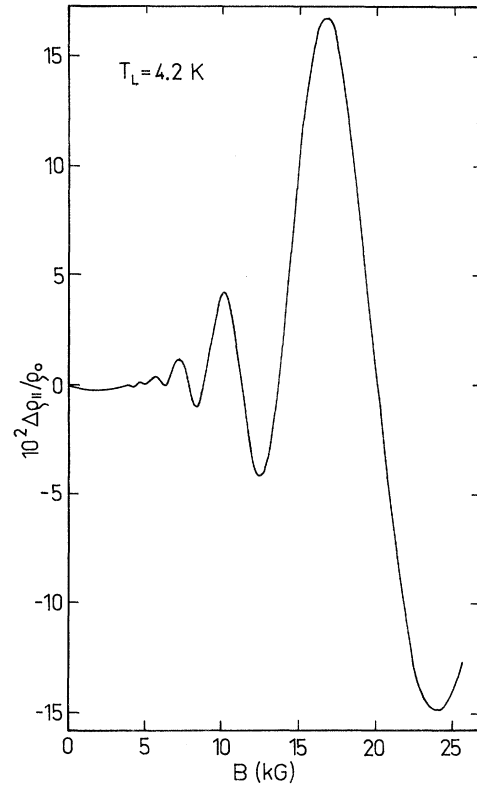


FIG. 5. Longitudinal magnetoresistance for magnetic fields up to 25 kG at 4.2 K.

were obtained from the measurement of the transverse magnetoresistance under Ohmic conditions. The slope of the dashed line yields the same value

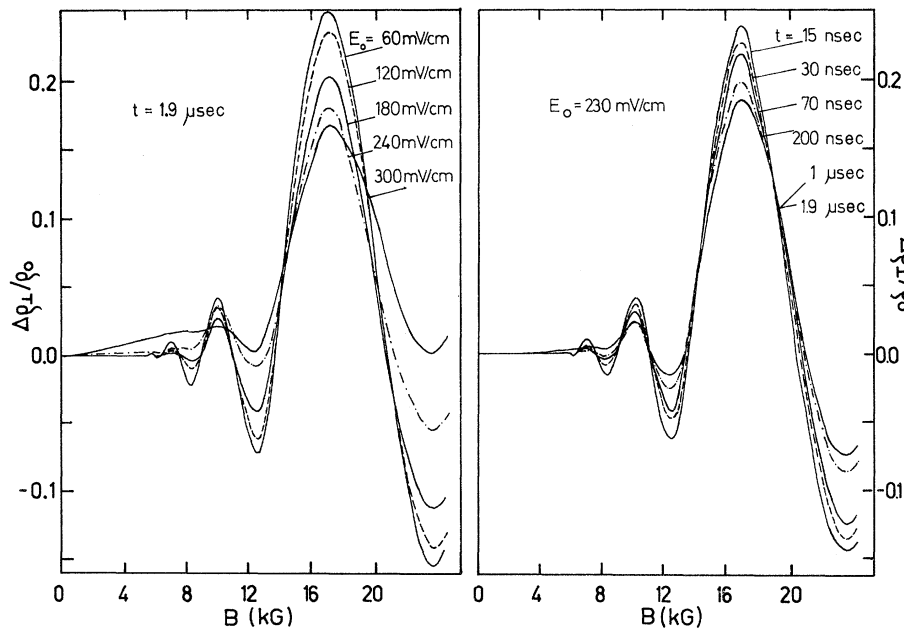


FIG. 6. Magnetic field dependence of the transverse magnetoresistance at 4.2 K; left-hand side: for different electric fields between 60 and 300 mV/cm at a time of 1.9 μ sec after application of the voltage pulse; right-hand side: for different times after application of an electric field of 230 mV/cm.

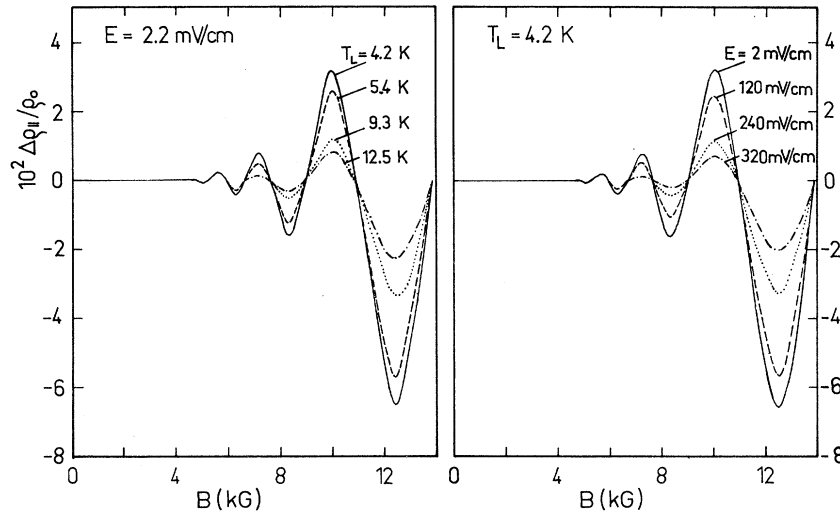


FIG. 7. Oscillatory component of the longitudinal magnetoresistance; left-hand side: measurement under Ohmic conditions and different lattice temperatures between 4.2 and 12.5 K; right-hand side: measurements at a constant lattice temperature of 4.2 K and different electric fields between 2 and 320 mV/cm.

of 7.0 for the Dingle temperature.

The method for determining the dependence of the electron temperature on the electric field strength is shown in Fig. 9. On the left-hand side the ratio of the amplitude A at an elevated temperature T to the amplitude A_0 at the reference temperature T_0 , which was 4.2 K in our case, is plotted vs temperature for a certain magnetic field strength. This dependence can either be obtained experimentally as shown in Fig. 7 or derived theoretically by means of Eq. (10). On the right-hand side the ratio of the amplitude A for a certain elec-

tric field to the amplitude A_0 under Ohmic conditions is plotted vs the applied electric field for the same magnetic field. The dashed line correlates an electron temperature of 8 K to an electric field of 200 mV/cm.

This procedure was done for a large number of electric fields up to approximately 300 mV/cm and for measurements in the longitudinal as well as in the transverse configuration. For magnetic fields below 12 kG, no detectable difference in the electron temperatures deduced from both configurations was observed. Moreover, the temperatures deduced from the decrease of the amplitudes at different magnetic fields were essentially the same. The variation of the electron temperature with electric field up to 300 mV/cm is shown in Fig.

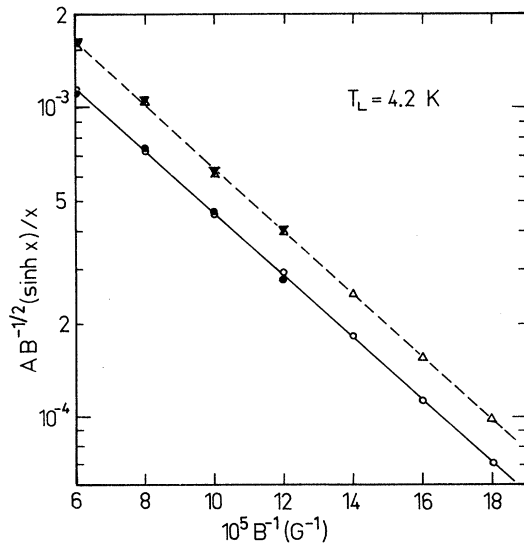


FIG. 8. Determination of the Dingle temperature; open circles: from the Ohmic longitudinal magneto-resistance of Fig. 5; full circles: from the longitudinal magnetoresistance at 200 mV/cm; open triangles: from Ohmic transverse magnetoresistance; full triangles: from transverse magnetoresistance at 200 mV/cm.

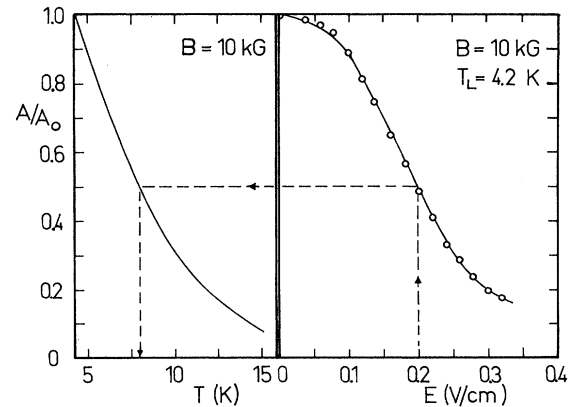


FIG. 9. Determination of the electron temperature which corresponds to a certain electric and magnetic field; left-hand side: variation of the normalized amplitude at a certain magnetic field with temperature; right-hand side: dependence of the amplitude of an oscillation on the electric field at a field at a fixed lattice temperature.

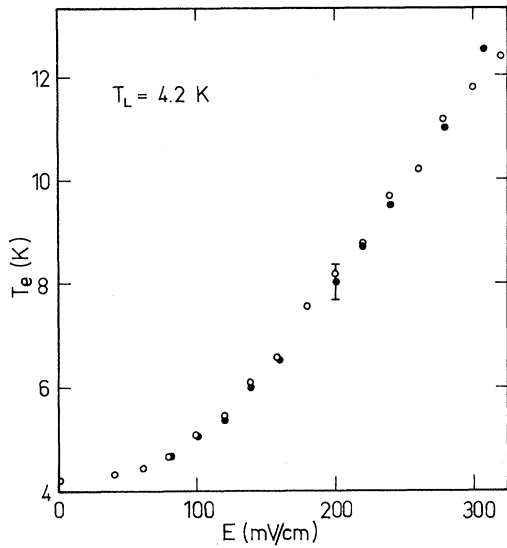


FIG. 10. Dependence of the electron temperature on the electric field at a lattice temperature of 4.2 K; open circles: data from longitudinal magnetoresistance; full circles: data from the transverse magnetoresistance.

10. The values were taken from the SdH amplitudes at 1.9 μ sec after the application of the voltage pulse; the conditions were already stationary after 1 μ sec.

As indicated in Fig. 6, the time-dependent measurements yielded information on the variation of T_e with time after application of the voltage pulse. In Fig. 11, the electron temperature is plotted vs time after application of the pulse for different electric fields of 100, 185, and 230 mV/cm.

The assumption of a constant Dingle temperature which was used in the evaluation of the electron temperature is justified for several reasons. The Dingle temperature is closely related to the mobility temperature³² T'_μ defined by $T'_\mu = \hbar e / (\pi k m \mu)$, which was 7.45 K in our case. Since the mobility temperature is constant up to 300 mV/cm within 2%, it is reasonable to assume that the Dingle temperature also does not vary. Furthermore, it is possible to deduce the Dingle temperature from the SdH amplitudes at higher electric fields after having determined the electron temperature by the above-outlined procedure. This was done for an electric field of 200 mV/cm for the longitudinal (full circles in Fig. 8) as well as for the transverse configuration (full triangles in Fig. 8). From the fact that the data points coincide within experimental error with the points obtained from the measurement at 4.2 K under Ohmic conditions we draw the following conclusions: (i) The electron temperatures are determined correctly and do not depend on the magnetic field and (ii) the Dingle temperature corresponding to the slope of the plot in

Fig. 8 does not vary with applied electric field.

Using Eqs. (8) and (9), we have calculated the oscillatory part of the longitudinal magnetoresistance for temperatures of 8 and 12 K and compared it with experimental data for electric fields of 200 and 305 mV/cm, respectively. The result is shown in Fig. 12. Values of $T_D = 7.0$ K, $\nu = 0$, and $s = 5$ were used in the calculation. The excellent agreement which was obtained without any adjustable parameters justifies the use of the electron temperature T_e in the description of the influence of an electric field on the electron distribution in this case. The same result can also be drawn from Fig. 7, where a 1:1 correspondence between the experiment under Ohmic conditions at different lattice temperatures above 4.2 K and under hot-electron conditions at a fixed lattice temperature has been found experimentally.

The SdH theory predicts a difference between the amplitudes in the transverse and longitudinal configuration by a factor of 2.5. From the data of Fig. 8, we have found that the amplitude of the transverse oscillations is only a factor of about 1.5 higher than those of the longitudinal oscillations, independent of the electron temperature. This factor was already obtained by other authors from measurements of the Ohmic SdH effect in *n*-InAs.^{33,34}

D. Nonoscillatory Magnetoresistance

In the magnetic field region below 5 kG, we have found a negative magnetoresistance. Its temperature dependence was studied between 2.4 and 4.2 K. Figure 13 shows the transverse magnetoresistance for different lattice temperatures. At 2.4

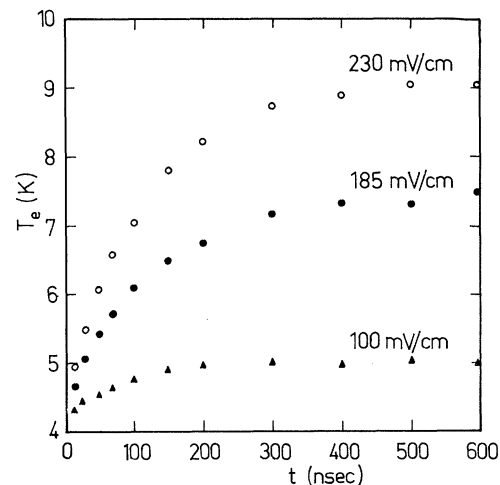


FIG. 11. Dependence of the electron temperature on the time after application of the voltage pulse; triangles: for an electric field $E = 100$ mV/cm; full circles: $E = 185$ mV/cm; open circles: $E = 230$ mV/cm.

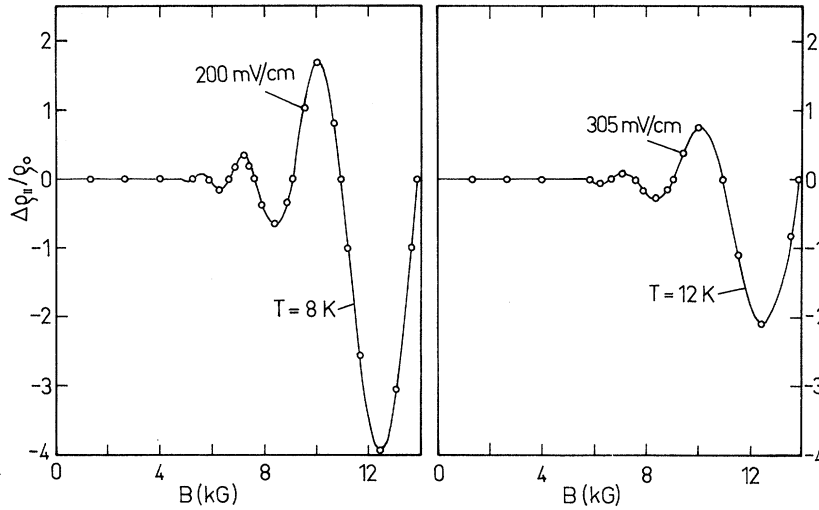


FIG. 12. Oscillatory part of the longitudinal magnetoresistance; full curves: theory for 8 and 12 K; open circles: data from the experiment at 200 and 305 mV/cm, respectively, taken at 4.2 K.

K, we have observed a value of -3.7×10^{-3} at 2 kG, which decreases with increasing lattice temperature.

In InAs, the region where the resistance variation follows a B^2 dependence is a very narrow one similar to the experimental results in InSb.²⁴ As can be seen from Fig. 14, the negative magnetoresistance is proportional to B^2 only up to 100 G. For higher magnetic fields it also can not be described by the Brillouin function.²¹ Therefore we did not deduce from our measurements a characteristic temperature according to a Curie-Weiss law. It was already pointed out by Halbo and Sladek²³ that the Toyozawa model also could not account for the experimental data in degenerate *n*-GaAs.

An alternative description of the negative magnetoresistance was proposed by Khosla and Fisher²⁸ by the expression given in Eq. (14). With the coefficients B_1 and B_2 listed in Table I we have obtained the fit of this relation to the experimental data shown in Fig. 15. Since the coefficients B_1 and B_2 are functions of various parameters such as exchange integrals and spin-splitting factors,

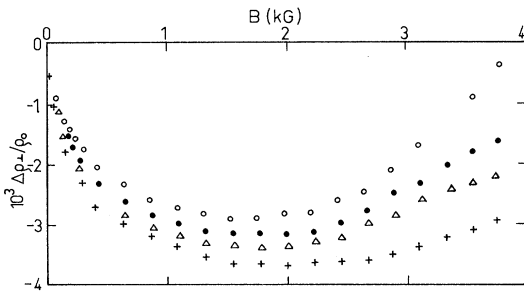


FIG. 13. Dependence of the negative magnetoresistance on the magnetic field; open circles: $T_L = 4.2$ K; full circles: $T_L = 3.05$ K; triangles: $T_L = 2.8$ K; crosses: $T_L = 2.4$ K.

which are unknown in our case, no further analysis can be made at present.

The influence of an electric field on the nonoscillatory part of the magnetoresistance was also studied for a lattice temperature of 4.2 K. The application of an electric field causes an increase of the positive component as shown in Fig. 16 for different electric fields up to 860 mV/cm. The time-dependent behavior is shown in Fig. 17 for times between 30 nsec and 1 μ sec after application of a constant-voltage pulse equivalent to an electric field of 1 V/cm.

Unfortunately there is no possibility for a quantitative comparison of the nonoscillatory positive magnetoresistance with the theoretical expression

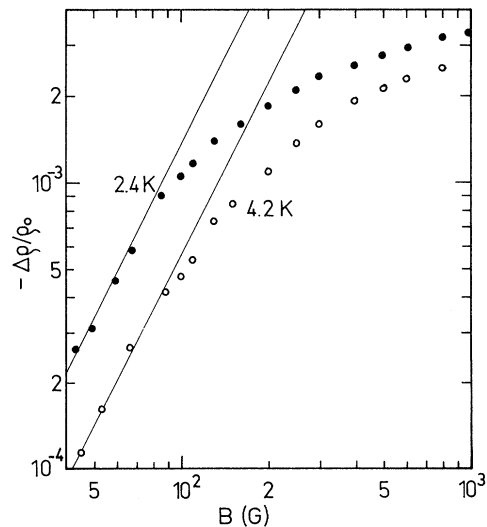


FIG. 14. Negative magnetoresistance as a function of magnetic field on a logarithmic scale. Full circles: $T_L = 2.4$ K; open circles: $T_L = 4.2$ K. Only below approximately 100 G is a B^2 dependence found.

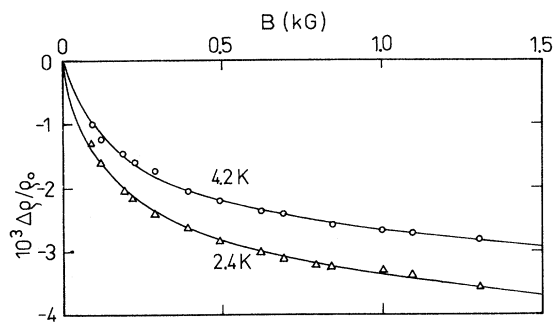


FIG. 15. Comparison of the experimental data of the negative magnetoresistance with calculated ones; circles: $T_L = 4.2$ K; triangles: $T_L = 2.4$ K; full curves: calculated with Eq. (14) and constants of Table I.

of Eq. (15). Because of the high mobility of the investigated samples, the range of validity of Eq. (15) is restricted to magnetic fields well below 4 kG. At these magnetic fields the magnetoresistance is a superposition of a negative and a positive component which cannot be separated easily. Qualitatively, the results presented in Figs. 16 and 17 fit well to a model where the electron temperature increases with the electric field and with time after application of the voltage pulse.

V. DISCUSSION

In order to determine the dominant energy-loss mechanisms we have performed calculations of the energy-loss rates and their dependences on the electron temperature for deformation potential scattering, piezoelectric scattering, and scattering by polar optical phonons. The effect of the nonpara-

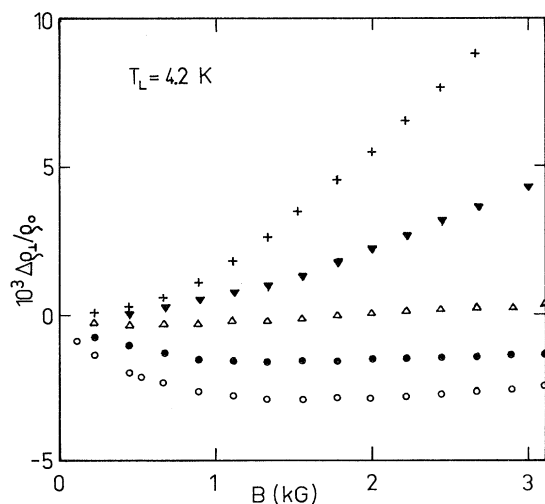


FIG. 16. Variation of the nonoscillatory magnetoresistance with electric field; circles: $E = 10$ mV/cm; full circles: 150 mV/cm; open triangles: 220 mV/cm; full triangles: 440 mV/cm; crosses: 860 mV/cm.

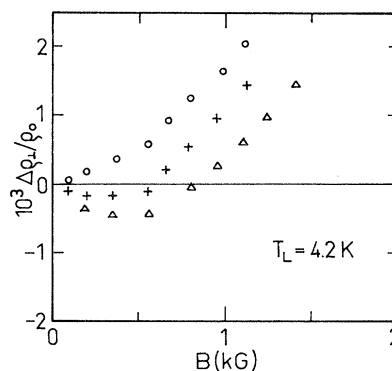


FIG. 17. Dependence of the magnetoresistance on the time after application of a voltage pulse corresponding to a field of 1 V/cm; triangles: 30 nsec after the rise of the pulse; crosses: 100 nsec; circles: 1 μ sec.

bolicity of the conduction band on the transport in InAs was studied by Curby and Ferry³⁵ for non-degenerate statistics. For the sake of simplicity we have ignored the nonparabolicity in our calculations but have taken into account the degeneracy of the electron gas. Using Eqs. (17) and (19) and Eqs. (18) and (20), the energy-loss rates were obtained for screened piezoelectric scattering and screened deformation potential scattering, respectively. The result is given in Fig. 18. The dashed curve holds for piezoelectric scattering with a coupling constant $e_{14}^2 = 1.82 \times 10^8$ dyn/cm² deter-

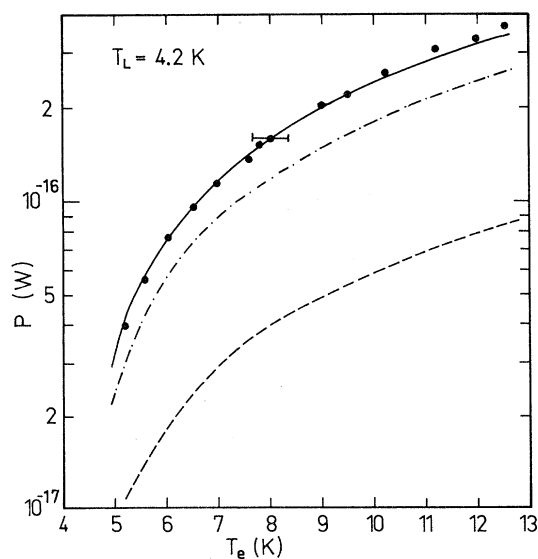


FIG. 18. Dependence of the energy-loss rate P on the electron temperature; dashed curve: theory for screened piezoelectric interaction; dash-dotted curve: theory for screened deformation potential scattering with $E_c = 4.05$ eV; full curve: combination of both contributions; circles: experimental data taken from Fig. 10.

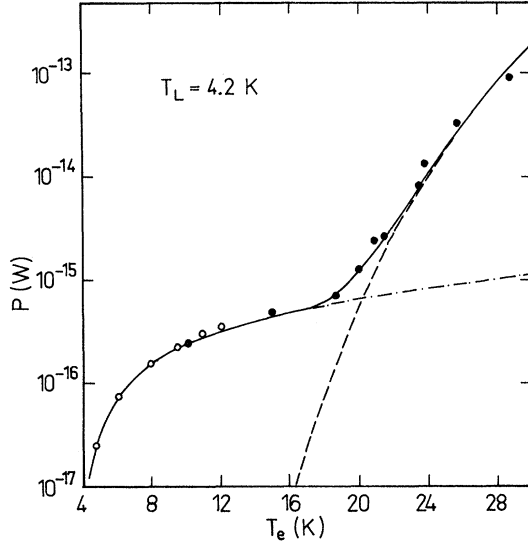


FIG. 19. Dependence of the energy-loss rate P on the electron temperature; dashed curve: energy-loss rate due to polar-optical scattering; dash-dotted curve: energy-loss rate due to both types of screened acoustic scattering; full curve: total-energy-loss rate; open circles: data obtained from SdH measurements; full circles: data obtained from mobility measurements.

mined by Arlt and Quadflieg.³⁶ The dash-dotted curve is valid for screened deformation potential scattering. Since the deformation potential constant of the conduction band of InAs is not known very well, we have used it as an adjustable parameter to fit the sum of the energy-loss rates for both types of acoustic scattering to the experimental data in Fig. 18; these data are a plot of the product $e\mu E^2$ vs the electron temperature determined from the decrease of the SdH amplitudes. A best fit, represented by the solid line in Fig. 18, was obtained with a value of $E_c = 4.05 \pm 0.25$ eV. For comparison, Rode³⁷ has given a value of $E_c = 4.97$ eV.

At temperatures above 18 K, the emission of polar optical phonons becomes an effective energy-loss mechanism. In Fig. 19, the theoretical energy-loss rate for polar optical scattering calculated with Eq. (24) is plotted vs the electron temperature (dashed curve). The dash-dotted curve represents the calculation of the sum of the energy-loss rates due to both types of acoustic scattering. The con-

TABLE I. Values of the parameters to fit the expression $\Delta\rho/\rho_0 = -B_1 \ln[1 + B_2(T)B^2]$.

Temp. (K)	B_1 (10^{-4})	B_2 (10^{-3} G^{-2})
4.2	3.48	2.12
2.4	4.06	4.13

stants used in the numerical calculations are listed in Table II. The full curve was obtained by simply adding the contributions of all three scattering mechanisms. The experimental data of Fig. 19 are again a plot of the product $e\mu E^2$ vs the electron temperature, where T_e for the open circles was obtained from the SdH effect and for the full circles from a comparison of the $\mu(E)$ and $\mu(T_L)$ curves.

Finally, we have calculated the dependence of the electron temperature and the mobility on the electric field. For different values of the reduced Fermi energy η we have calculated the corresponding electron temperature from the relation

$$n = 4\pi \left(\frac{2mkT_e}{h^2} \right)^{3/2} F_{1/2} \left(\frac{\epsilon_F}{kT_e} \right), \quad (25)$$

the mobility $\mu(T_e)$ by means of Eq. (1), and the total-energy-loss rate $\langle P_{\text{tot}} \rangle$:

$$\langle P_{\text{tot}}(T_e) \rangle = \langle P_{\text{pl}}(T_e) \rangle + \langle P_{\text{def}}(T_e) \rangle + \langle P_{\text{po}}(T_e) \rangle. \quad (26)$$

Once the mobility and the total-energy-loss rate are known, the electric field which corresponds to this electron temperature is given by

$$E(T_e) = \left(\frac{\langle P_{\text{tot}}(T_e) \rangle}{e\mu(T_e)} \right)^{1/2}. \quad (27)$$

The result of the calculation is shown in Fig. 20, where the full line represents the mobility and the dashed line the electron temperature vs electric field. The triangles indicate measured values of

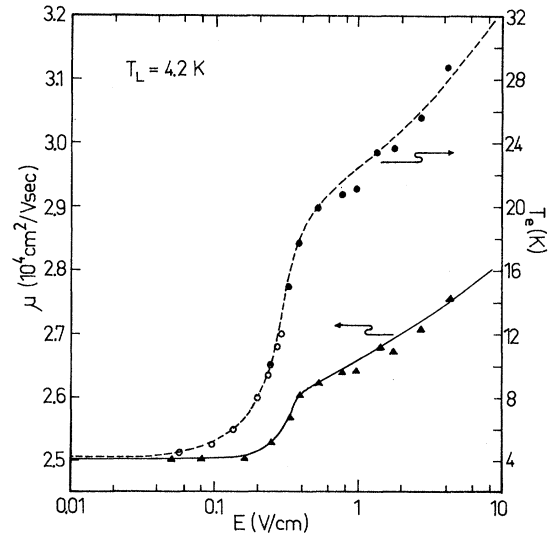


FIG. 20. Dependence of the mobility and the electron temperature on the electric field; triangles: measured mobility variation; full curve: calculated dependence; open circles: electron temperature deduced from SdH measurements; full circles: electron temperatures deduced from mobility measurements; dashed curve: calculated electron temperatures.

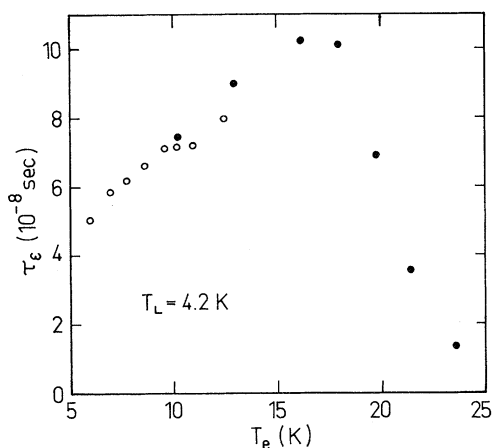


FIG. 21. Variation of the phenomenological energy relaxation time with electron temperature; open circles: experimental data from SdH measurements; full circles: experimental data from mobility measurements.

the mobility. The electron temperatures were either taken from the field-dependent SdH effect (open circles) or from the comparison of the $\mu(T_L)$ and $\mu(E)$ curves (full circles). Between 200 and 300 mV/cm, data obtained by both methods are in satisfactory agreement. The kink in both curves at approximately 500 mV/cm is obviously caused by the onset of polar-optical-phonon emission. From the coincidence of the experimental points and the theoretical curves we conclude that up to 30 K the electron-temperature model is a reasonable description of the non-Ohmic transport. Above 30 K, deviations of the experimental data and the theoretical calculation occurred, which are probably caused by the fact that at higher temperatures the Fermi-Dirac distribution function overestimates the energy loss due to the emission of polar optical phonons, thereby making the electron-temperature model no longer a good approximation.

Although no energy relaxation time exists in the rigorous meaning for polar optical scattering, it is useful to define a phenomenological quantity τ_e by

$$\frac{d\langle\epsilon\rangle}{dt} = -\frac{\langle\epsilon(T_e)\rangle - \langle\epsilon(T_L)\rangle}{\tau_e} + e\mu E^2, \quad (28)$$

The brackets indicate the average of the energy with respect to the distribution function. In a degenerate semiconductor the mean energy as a function of temperature is given by

$$\langle\epsilon(T)\rangle = \frac{kT F_{3/2}(\eta)}{F_{1/2}(\eta)}. \quad (29)$$

Figure 21 shows the variation of τ_e with electron temperature obtained with aid of Eq. (28) from the SdH measurements (open circles) as well as from the mobility measurements (full circles) under

equilibrium conditions. Up to 18 K, where acoustic scattering dominates the energy loss, τ_e increases with T_e , whereas it decreases rapidly as polar optical scattering becomes effective. The maximum of τ_e occurring at 18 K has a value of approximately 100 nsec. Therefore in the electric field range 200–700 mV/cm a time-dependent variation of the mobility is expected to be observable. The experimental evidence for this was given in Fig. 3. Since the variation is too small to derive directly the energy relaxation time as was done for the case of InSb by Maneval *et al.*,⁶ the utility of the time-dependent SdH measurements of Fig. 6 is again demonstrated. Further, it is possible to deduce values of τ_e from the time dependence of T_e given in Fig. 11 using Eq. (28). These values are in good agreement with the values plotted in Fig. 21 which were obtained from stationary conditions at the end of a 2- μ sec pulse.

We want to point out that the determination of the electron temperature from the decrease of the SdH amplitudes requires a quantizing magnetic field. The calculations of the energy-loss rates described in this section, which we have compared with SdH data, should therefore take into account the influence of the magnetic field. Unfortunately no theory of the energy-loss rate of a degenerate electron gas has been developed so far for a quantizing magnetic field under conditions where several Landau levels are occupied. From our experiments we conclude that the electron temperature and consequently the energy loss do not depend significantly on the magnetic field under these conditions. We have therefore used the expressions given by Kogan³⁰ for the energy-loss rates, which do not include a magnetic field.

VI. CONCLUSIONS

Two methods have been employed to determine experimentally the electron temperature as a function of the electric field. For the case of strong degeneracy the observation of the SdH effect dependent on the applied electric field is a useful tool to determine electron temperatures and to re-

TABLE II. Constants used in the numerical calculation.

$m = 0.023m_0$	Effective mass ^a
$d = 5.66 \text{ g/cm}^3$	Mass density
$e_{14}^2 = 1.82 \times 10^8 \text{ dyn/cm}^2$	Piezoelectric modulus ^b
$\Theta = 350 \text{ K}$	Debye temperature ^c
$\kappa = 14.55$	Static dielectric constant ^d
$\kappa_\infty = 11.80$	Optical dielectric constant ^d
$E_0 = 2116 \text{ V/cm}$	Polar-optical coupling constant ^e

^aReference 38.

^bReference 36.

^cReference 37.

^dReference 39.

^eSee text.

solve their time-dependent increase. At higher fields, where the electrons are heated appreciably and the degeneracy decreases, the mobility changes become larger and can be used for a determination of the electron temperature if impurity scattering dominates the momentum relaxation process. In principle, also the variation of the nonoscillatory positive magnetoresistance with electric field should give information about the electron temperature. Unfortunately the negative magnetoresistance at low magnetic fields competes with the positive component and at the present state of theory a reliable separation of both contributions is not yet possible.

We have compared the experimentally obtained temperature dependence of the energy-loss rate with theoretical calculations. From this comparison we have deduced the relative strength of both types of screened acoustic scattering and have determined a value of the deformation potential constant of $E_c = 4.05 \pm 0.25$ eV. At an electron tem-

perature of approximately 18 K the emission of polar optical phonons becomes effective and causes a change in the slope of the $T_e(E)$ and $\mu(E)$ curves, which we were able to explain quantitatively up to an electric field of 10 V/cm. The relatively large values of the energy relaxation time of about 50–100 nsec cause a time dependence of the current-density–field-strength characteristic and allow a direct observation of the increase in the electron temperature by a measurement of the time-dependent decrease of the SdH amplitudes.

ACKNOWLEDGMENTS

We thank Professor K. Seeger for his continuous interest in this work, Dr. H. Heinrich and Dr. K. Hess for valuable discussions, and Dr. H. Kuzmany and Dr. M. W. Valenta for a critical reading of the manuscript. Numerical calculations were done at the Institut für Numerische Mathematik, T. H., Vienna.

†Work supported by the "Fonds zur Förderung der wissenschaftlichen Forschung," Austria, and the Ludwig Boltzmann Gesellschaft, Austria.

¹For a review see E. M. Conwell, in *Solid State Physics*, edited by F. Seitz, D. Turnbull, and H. Ehrenreich (Academic, New York, 1967), Suppl. 9.

²R. J. Sladek, *Phys. Rev.* **120**, 1589 (1960).

³T. M. Lifshits, A. Ya. Oleinikov, and A. Ya. Shulman, *Phys. Status Solidi* **14**, 511 (1966).

⁴M. A. Kinch, *Proc. Phys. Soc. (London)* **90**, 819 (1967).

⁵H. Miyazawa, *J. Phys. Soc. Japan* **26**, 700 (1969).

⁶J. P. Maneval, A. Zylbersztejn, and H. F. Budd, *Phys. Rev. Letters* **23**, 848 (1969).

⁷J. J. Whalen and C. R. Westgate, *Appl. Phys. Letters* **15**, 292 (1969).

⁸W. Szymanska and J. P. Maneval, *Solid State Commun.* **8**, 879 (1970).

⁹J. P. Martin and J. B. Mead, *Appl. Phys. Letters* **17**, 320 (1970).

¹⁰D. J. Oliver, *Phys. Rev.* **127**, 1045 (1962).

¹¹R. S. Crandall, *Phys. Rev. B* **1**, 730 (1970).

¹²R. S. Crandall, *J. Phys. Chem. Solids* **31**, 771 (1970).

¹³R. Stratton, *Proc. Roy. Soc. (London)* **A246**, 406 (1958).

¹⁴R. A. Isaacson and F. Bridges, *Solid State Commun.* **4**, 635 (1966).

¹⁵J. Konopka, *Solid State Commun.* **5**, 809 (1967).

¹⁶G. Bauer and H. Kahlert, in *Proceedings of the International Conference on the Physics of Semiconductors*, Cambridge, Mass., 1970, edited by S. P. Keller, J. C. Hensel, and F. Stern (U.S. Atomic Energy Commission, Oak Ridge, Tenn., 1970).

¹⁷A. C. Beer, in *Solid State Physics*, edited by F. Seitz and D. Turnbull (Academic, New York, 1963), Suppl. 4, p. 111.

¹⁸E. N. Adams and T. D. Holstein, *J. Phys. Chem. Solids* **10**, 254 (1959).

¹⁹P. N. Argyres, *J. Phys. Chem. Solids* **4**, 19 (1959).

²⁰R. Kubo, S. J. Miyake, and W. Hashitsume, in *Solid State Physics*, edited by F. Seitz, D. Turnbull, and M. Ehrenreich (Academic, New York, 1965), Vol. 17, p. 269, Appendix A.

²¹W. Sasaki, *J. Phys. Soc. Japan Suppl.* **21**, 543 (1966).

²²M. Balkanski and A. Giesmar, *J. Phys. Soc. Japan Suppl.* **21**, 554 (1966).

²³L. Halbo and R. J. Sladek, *Phys. Rev.* **173**, 794 (1968).

²⁴Y. Katayama and S. Tanaka, *Phys. Rev.* **153**, 873 (1967).

²⁵Y. Toyozawa, *J. Phys. Soc. Japan* **17**, 986 (1962).

²⁶K. Yosida, *Phys. Rev.* **107**, 396 (1957).

²⁷L. A. Kaufman and L. J. Neuringer, *Phys. Rev. B* **2**, 1840 (1970).

²⁸R. P. Khosla and J. R. Fischer, *Phys. Rev. B* **2**, 4084 (1970).

²⁹R. F. Greene, *J. Electron. Control* **3**, 387 (1957).

³⁰Sh. M. Kogan, *Fiz. Tverd. Tela* **4**, 2474 (1962) [*Sov. Phys. Solid State* **4**, 1813 (1963)].

³¹N. V. Zotova, T. S. Lagunova, and D. N. Nasledov, *Fiz. Tverd. Tela* **5**, 3329 (1961) [*Sov. Phys. Solid State* **5**, 2439 (1964)].

³²L. M. Roth and P. N. Argyres, in *Semiconductors and Semimetals*, edited by R. K. Willardson and A. C. Beer (Academic, New York, 1966), Vol. 1, p. 159.

³³R. J. Sladek, *Phys. Rev.* **110**, 817 (1958).

³⁴M. S. Bresler, N. A. Redko, and S. S. Shalyt, *Phys. Status Solidi* **15**, 745 (1966).

³⁵R. C. Curby and D. K. Ferry, *Phys. Rev. B* **3**, 3379 (1971).

³⁶G. Arlt and P. Quadflieg, *Phys. Status Solidi* **25**, 323 (1968).

³⁷D. L. Rode, *Phys. Rev. B* **2**, 1012 (1970).

³⁸M. Balkanski and E. Amzallag, *Phys. Status Solidi* **30**, 407 (1968).

³⁹M. Hass, in *Semiconductors and Semimetals*, edited by R. K. Willardson and A. C. Beer (Academic, New York, 1967), Vol. 3, p. 14.